

Sub-15-fs X-ray pump and X-ray probe experiment for the study of ultrafast magnetization dynamics in ferromagnetic alloys

Xuan Liu, Alaaeldine Merhe, Emmanuelle Jal, Renaud Delaunay, Romain Jarrier, Valentin Chardonnet, Marcel Hennes, Sorin Chiuzbaian, Katherine Légaré, Martin Hennecke, et al.

▶ **To cite this version:**

Xuan Liu, Alaaeldine Merhe, Emmanuelle Jal, Renaud Delaunay, Romain Jarrier, et al.. Sub-15-fs X-ray pump and X-ray probe experiment for the study of ultrafast magnetization dynamics in ferromagnetic alloys. Optics Express, 2021, 29 (20), pp.32388. 10.1364/OE.430828 . hal-03808361

HAL Id: hal-03808361
https://hal.science/hal-03808361

Submitted on 14 Oct 2022

HAL is a multi-disciplinary open access archive for the deposit and dissemination of scientific research documents, whether they are published or not. The documents may come from teaching and research institutions in France or abroad, or from public or private research centers.

L'archive ouverte pluridisciplinaire **HAL**, est destinée au dépôt et à la diffusion de documents scientifiques de niveau recherche, publiés ou non, émanant des établissements d'enseignement et de recherche français ou étrangers, des laboratoires publics ou privés.

Research Article | Vol. 29, No. 20 / 27 Sep 2021 / Optics Express 32388
Optics EXPRESS

Sub-15-fs X-ray pump and X-ray probe experiment for the study of ultrafast magnetization dynamics in ferromagnetic alloys

XUAN LIU,[1] ALAAELDINE MERHE,[1] EMMANUELLE JAL,[1] RENAUD DELAUNAY,[1] ROMAIN JARRIER,[1] VALENTIN CHARDONNET,[1] MARCEL HENNES,[1] SORIN G. CHIUZBAIAN,[1] KATHERINE LÉGARÉ,[2] MARTIN HENNECKE,[3] ILIE RADU,[3,4] CLEMENS VON KORFF SCHMISING,[3] SÆREN GRUNEWALD,[5] MARION KUHLMANN,[5] JAN LÜNING,[1,6] AND BORIS VODUNGBO[1,*]

[1]*Sorbonne Université, CNRS, Laboratoire de Chimie Physique-Matière et Rayonnement, 75005 Paris, France*
[2]*Institut National de la Recherche Scientifique, Centre Énergie Matériaux et Télécommunications, 1650 Boulevard Lionel-Boulet, Varennes, Québec, J3X 1S2, Canada*
[3]*Max Born Institut für Nichtlineare Optik und Kurzzeitspektroskopie, 12489 Berlin, Germany*
[4]*Currently with Department of Physics, Free University Berlin, Arnimallee 14, 14195, Berlin, Germany*
[5]*Deutsches Elektronen-Synchrotron, 22607 Hamburg, Germany*
[6]*Currently with Helmholtz-Zentrum Berlin für Materialien und Energie, 14109 Berlin, Germany*
[*]*boris.vodungbo@sorbonne-universite.fr*

Abstract: In this paper, we present a new setup for the measurement of element-specific ultrafast magnetization dynamics in ferromagnetic thin films with a sub-15-fs time resolution. Our experiment relies on a split and delay approach which allows us to fully exploit the shortest X-rays pulses delivered by X-ray Free Electrons Lasers (close to the attosecond range), in an X-ray pump – X-ray probe geometry. The setup performance is demonstrated by measuring the ultrafast elemental response of Ni and Fe during demagnetization of ferromagnetic Ni and $Ni_{80}Fe_{20}$ (Permalloy) samples upon resonant excitation at the corresponding absorption edges. The transient demagnetization process is measured in both reflection and transmission geometry using, respectively, the transverse magneto-optical Kerr effect (T-MOKE) and the Faraday effect as probing mechanisms.

© 2021 Optical Society of America under the terms of the OSA Open Access Publishing Agreement

1. Introduction

A few years ago, the question arose whether nickel and iron would display different ultrafast demagnetization dynamics in Py ($Ni_{80}Fe_{20}$) upon excitation with femtosecond laser pulses and whether this magnetization quenching would differ from the one observed in the pure materials. Mathias *et al.* [1].and Jana *et al.* [2]. found quite similar demagnetization dynamics for Ni and Fe in Py by using a near infrared (NIR) pump and an element-specific high order harmonic (HHG) probe in a transverse magneto-optic Kerr effect (T-MOKE) geometry : they claimed that Fe is demagnetizing faster than Ni with a small delay (~10 fs) between the onset of their two dynamics. However, using a NIR pump and a soft X-ray probe, exploiting the X-ray circular dichroism (XMCD) at the *L* absorption edge at the femto-slicing beamline of the BESSY II synchrotron of Helmholtz Zentrum Berlin, Radu *et al*. [3] observed that Ni and Fe have very different magnetization dynamics in a Py sample, and that Ni is faster than Fe.

To study the above question in more detail and understand this discrepancy, a very good time resolution (ideally shorter than 10 fs) and hence ultra-short pulses are required. Moreover, the need to specifically probe elements in an alloy calls for the use of an X-ray probe. More generally,

#430828 https://doi.org/10.1364/OE.430828
Journal © 2021 Received 2 Jun 2021; revised 19 Aug 2021; accepted 30 Aug 2021; published 24 Sep 2021

Optics EXPRESS

the solid-state ultrafast community need tools capable to resolve charge and spin dynamics with few femtoseconds/attoseconds time resolution and element specificity. This can be realized at attosecond high harmonics sources [4] but the low intensity of the latter seriously constrains the type of possible experiments.

At X-ray free-electron lasers (XFEL) recent developments now allow for the generation of few femtoseconds X-ray pulses [5,6] which have the potential to yield more versatile time-resolved spectroscopic experiments. Unfortunately, the traditional NIR pump – X-ray probe experimental schemes are typically limited by the pulse duration of the NIR laser, typically between 30 and 100 fs at XFEL facilities. The arrival time jitter between NIR and X-ray pulses further degrades the time resolution. It has to be noted that schemes have been developed at XFEL to produce several X-ray pulses separated by a variable delay to perform X-ray pump X-ray probe experiments [7,8,9]. These approaches have the advantages of getting rid of the jitter and of being theoretically only limited by the duration of the X-ray pulses. They also offer the powerful possibility to excite core electrons and can hence trigger dynamics that differ from those generated by NIR lasers. Unfortunately, those methods rely on XFEL special operation modes and are not widely available for users. Moreover, they have some limitations such as the range of delays accessible (typically between 0 and a few hundreds of femtoseconds).

Here, our goal is to fully exploit the very short X-ray pulses delivered at XFEL in an X-ray pump X-ray probe geometry to obtain a sub-15-fs time resolution with an easy-to-implement user-side setup. This is realized by splitting the X-ray beam into two parts: the first part is used to excite the sample and the second part is used to probe the sample state. In that way, we are only limited by the X-ray pulse duration. In this report, this enabled us to study the onset of the magnetization dynamics in Py with the best time resolution achievable at XFEL and to potentially resolve the fine details of the respective dynamics of the Fe and Ni sub-systems.

In the following, we describe the split and delay setup that we have designed, installed, and commissioned at the FLASH facility (DESY, Hamburg). At this source, the wavelength is easily tunable, thanks to a variable gap undulator which provides the possibility to probe magnetization dynamics for different transition metals elements. We show the results obtained on the Ni and Py systems in two different experimental geometries, reflection, and transmission respectively, using T-MOKE and Faraday effect as magnetization probe.

2. Split and delay setup

Our experimental setup (see Fig. 1) relies on a split and delay unit consisting of a flat rectangular mirror (120×20 mm^2), a fused silica ultra-flat substrate, and two spherical mirrors (focal length of about 1500 mm). The flat mirror (splitting mirror) is set at a grazing angle of 1.4° and geometrically splits the incoming beam (16 mm in diameter) into two parts. A major part of the XFEL intensity passes the mirror and reaches the first spherical mirror (pump mirror) which focuses the beam onto the sample: this constitutes the pump beam (purple). The reflected part reaches the second spherical mirror (probe mirror) and is also focused onto the sample: this constitutes the probe beam (orange). The angle between the two beams is 2.8°. Both pump and probe mirrors are coated with a wide band multilayer coating, four repetitions of Mo/Si purchased from AXO DRESDEN, reflecting XFEL radiation with at least 5% efficiency in the 52 eV – 67 eV photon energy range.

We keep the pump mirror fixed and control the spatial overlap by vertical and horizontal tilts of the focusing probe mirror. The position of the two beams is monitored by imaging the X-ray induced fluorescence of an yttrium aluminum garnet (YAG) screen positioned at the sample position with a CCD camera. In order to ensure that the two beams remain overlapped during the experiment, vibrations have to be kept at a minimum. Indeed, if we want to keep the positions of the two beams within 10 μm of their initial positions, the variations of the angle of incidence on each mirror has to be maintained below 10 μrad. This is achieved by using a low vibration

Optics EXPRESS

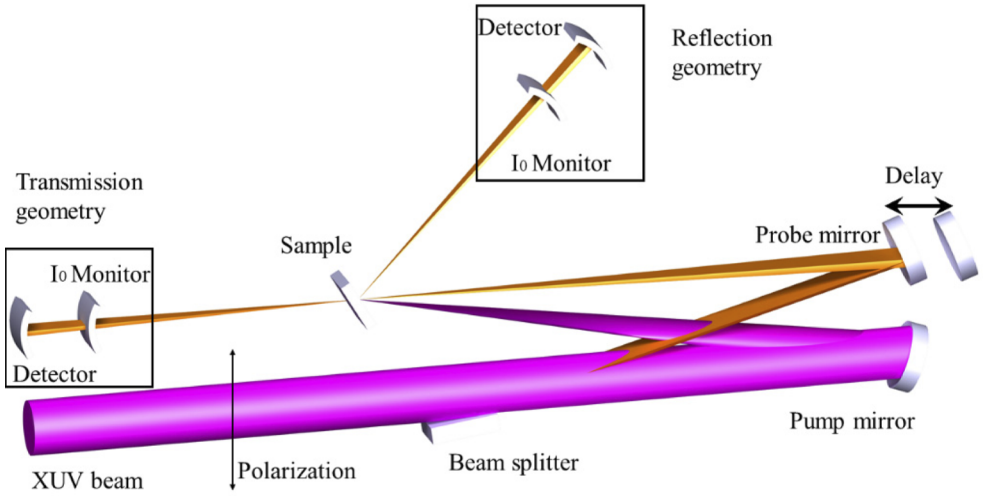


Fig. 1. Schematic diagram of the split and delay experimental setup. A flat rectangular mirror splits the XFEL beam into probe (in orange) and pump (in purple) parts which are each focused onto the sample by two spherical mirrors. The probe mirror is mounted on a motorized stage, which can be moved to introduce a time delay between the two branches. Reflection and transmission schemes can be implemented in our setup. For both geometries the incoming beam intensity, I_0, is measured by a semi-reflective mirror (a Si_3N_4 membrane) reflecting a fraction of the beam in an avalanche photodiode (APD) and the main signal is detected with another APD. The positions of the I_0 monitors (semi-reflective mirror and APD) and the detectors inside the black rectangles do not constitute an actual view of the setup. Figures 3 and 6 describe more accurately the positions of the different elements in the reflection and transmission geometries.

design for the mirror mounts and by isolating the vacuum chamber from any vibration source, especially from the vacuum pumps.

The time delay is changed by moving the probe mirror. The motorized stage used for this motion is set parallel to the probe mirror to sample direction: the properties of spherical mirrors ensure that the probe beam position remains stable while varying the delay. Moreover, the small alignment variations which may arise while scanning the delays can be corrected by the motorized rotations of the probe mirror (a correction table is recorded before the measurement). Since the beam impinges on the spherical mirrors at near normal incidence the delay changes amount to $2\times\Delta l/c$ where Δl is the position of the probe mirror compared to the zero-delay position and c the speed of light.

The probe beam can be focused down to a 50 µm spot, FWHM, (see Fig. 2(a)) on the sample and the size and pointing variations are negligible over the complete range of delays (about 10 ps or 1.5 mm). To homogeneously pump the sample, the pump beam focal spot has to be larger, about 100 µm, FWHM, (see Fig. 2(b)). This is easily achieved by using the mirror with the longest focal length for the pump. Indeed, the tolerance on the mirror curvature being of the order of 1%, there is a few millimeters difference between the focal lengths of the two mirrors. The profile of the beam also allows us to estimate roughly the pump fluence on the sample by taking into account the reflectivity of the different elements in the system. We can achieve a pump fluence of at most 2.5 mJ/cm^2 which is sufficient to demagnetize the different samples with an incoming XFEL pulse energy as low as 10 µJ. Contrary to NIR pump schemes, there is almost no reflectivity and 50 to 90% of the pump is absorbed by the magnetic layer (depending on its thickness and the exact photon energy).

Optics EXPRESS

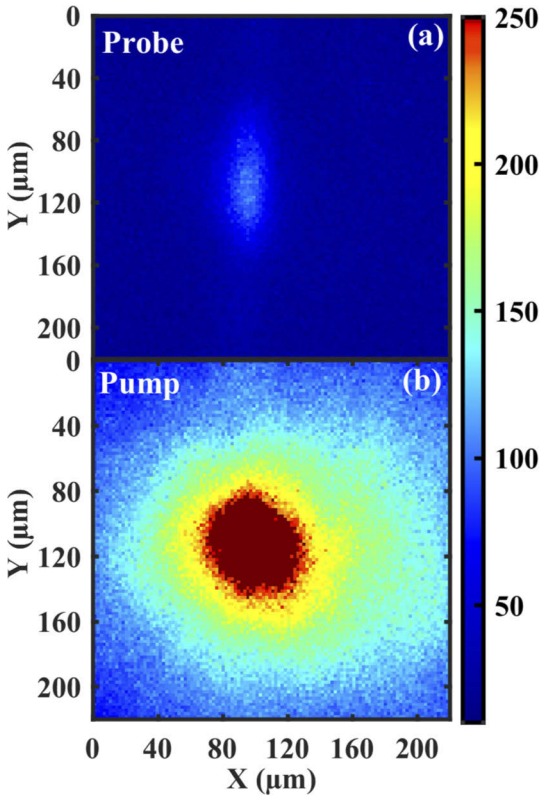


Fig. 2. Probe (a) and pump (b) beam profiles observed on a YAG crystal positioned at the sample position. Both images have the same color scales showing that the probe beam has a smaller footprint than the pump beam at the sample position. There is no visible change in the probe beam profile while changing the delay over a 10 ps range corresponding to a 1.5 mm motion of the probe mirror. This in line with the calculation of the Rayleigh length of the probe beam which is at least 3 mm long by conservatively considering the footprint of the probe beam on the focusing mirror to be half of the total incoming beam footprint (8 mm in diameter). In reality, the footprint is smaller leading to a longer Rayleigh length

3. Reflection geometry results

The first X-ray pump – X-ray probe experiments were realized in reflection geometry. We exploit the transverse magneto-optical Kerr effect (T-MOKE) to probe the magnetization of the sample. In this geometry, the sample is magnetized in plane and perpendicularly to the plane of incidence by an electromagnet delivering a maximum field of 20 mT (see Fig. 3), high enough to saturate the magnetization of the sample. The samples are set at an incidence angle of 45° to maximize the T-MOKE signal. Behind the sample, the probe beam intensity is detected with an avalanche photodiode (APD) while the pump beam (which is also partly reflected by the sample) is blocked by a beam stop. Before the sample, a semi-reflective mirror, consisting of a Si_3N_4 membrane capped with a very thin metallic layer, reflects part of the incoming beam to another APD to monitor the probe beam intensity.

We have studied two samples: a 10 nm thick Ni film and a 10 nm Py film. Both samples were grown on silicon substrates by magnetron sputtering on top of a buffer layer consisting of 5 nm of Ta and 5 nm of Pt. The samples were capped by a 10 nm Al layer to prevent oxidation. Because

Optics EXPRESS

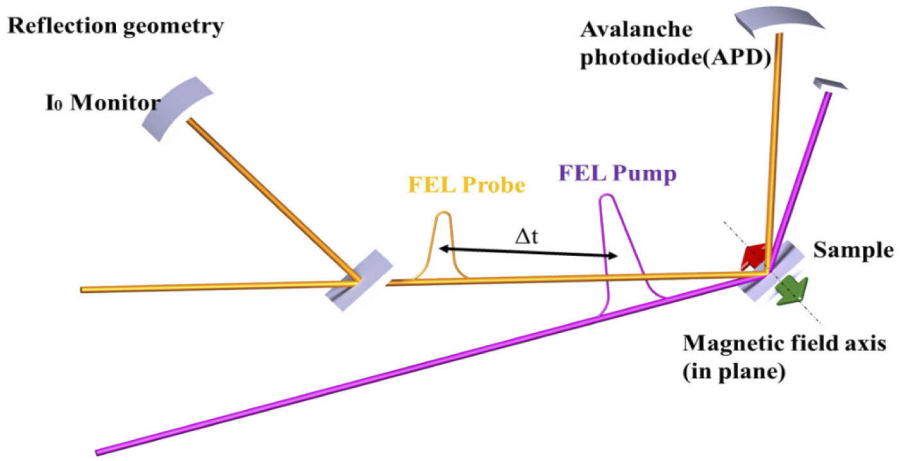


Fig. 3. Schematic description of the split and delay experimental setup in the reflection geometry showing the incidence angle on the sample (45°), the I_0 monitor, the direction of magnetization of the sample and the APD recording the reflected signal.

of the shape anisotropy, the sample can be easily magnetized in plane with a low magnetic field of less than 20 mT.

We performed our experiment at FLASH 2 on the beamline FL24. This XFEL delivers a train of pulses (up to a few hundred pulses per train but we typically used 20 to 80 for our experiments) separated by a few microseconds (typically 10 µs) at a 10 Hz repetition rate: this corresponds to 200 to 800 pulses per second. For this first experiment, we used a large pulse intensity of about 30 µJ to ensure that the pump fluence was sufficiently high. Consequently, the pulse duration could not be shorter than 20 fs. Each one of these pulses is split in two and constitutes one pump – probe event. For each time delay, we recorded several hundreds of these events for both magnetization directions. The field was continuously applied to the sample, in order to reset the magnetic state after each event. We also recorded the unpumped signal (by blocking the pump beam with an absorber mounted on a motorized translation stage) for both directions of the magnetization. We therefore acquired four signals for each delay.

Figure 4 (a) shows these four measurements as a function of the delay recorded at a photon energy of 66.7 eV, in resonance with the Ni $M_{2,3}$ absorption edges, obtained on the nickel sample [10]. We can clearly observe the T-MOKE effect since the reflected X-ray intensity shows large changes (factor ~2) upon flipping the external magnetic field (this particular photon-energy yielded the highest contrast). We can also observe the demagnetization effect on the two pumped curves: the signals displayed by these two curves get closer after time zero (the probe arrives after the pump for positive values of Δt). This demonstrates that the X-ray pump can efficiently trigger ultrafast demagnetization as it was assumed in a recent publication dealing with fluence dependence of X-ray magnetic scattering [11].

To better quantify the demagnetization, we have used the asymmetry parameter, which is defined as follows:

$$A = \frac{I_+^P - I_-^P}{I_+^P + I_-^P} \tag{1}$$

where I_+^P is the reflected intensity of p-polarized light with a positive magnetic field applied, while I_-^P corresponds to that with a negative magnetic field.

The asymmetry obtained with the pumped data clearly exhibits the classical behavior of ultrafast demagnetization with a reduction of the signal in the first few hundreds of femtoseconds followed by a slow recovery (see Fig. 4 (b)). The unpumped asymmetry shows a gradual decrease,

Optics EXPRESS

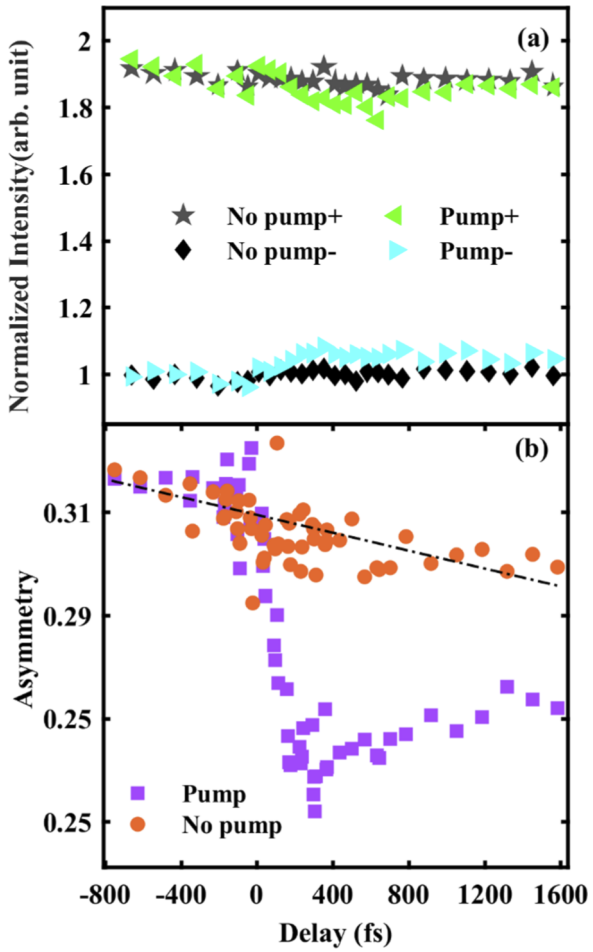


Fig. 4. (a) Reflectivity of the 10 nm Ni sample measured at a photon energy of 66.7 eV, in resonance with the $M_{2,3}$ absorption edges of Ni as a function of time delay (-800 to 1600 fs) in four different configurations: positive (green, left triangles), and negative (light blue, right triangles) magnetic field with pump laser; positive (grey, stars), and negative magnetic field (black, diamond) without pump laser. (b) Asymmetry calculated from these four curves for unpumped (orange, circle) and pumped (purple, square) configurations.

which is due to the slow contamination (carbon deposition) of the sample surface during the experiment. To correct for this effect, in the following the pumped asymmetry, A, will be divided by the unpumped asymmetry, A_0. This first measurement shows that the X-ray pump triggers a magnetic dynamic with a very similar behavior than the one induced by a NIR pump [12,13] and that our experimental setup works as expected.

We have also performed similar measurements on Py samples. Figure 5 shows the comparison between the magnetization dynamics, as revealed by the temporal evolution of the asymmetry parameter in these two samples. For both samples we observe a demagnetization followed by a partial recovery. The Ni sample demagnetizes about 5% more than the Py sample probably due to a combination of the following effects: (i) a higher absorption at this resonant photon energy due to a higher Ni content, (ii) a lower Curie temperature of pure Ni compared to the Py alloy (the Fe Curie temperature being much higher than that of Ni) and (iii) a higher magnetic moment for Fe [3]. We also observe that Py demagnetizes somewhat faster than pure Ni.

Optics EXPRESS

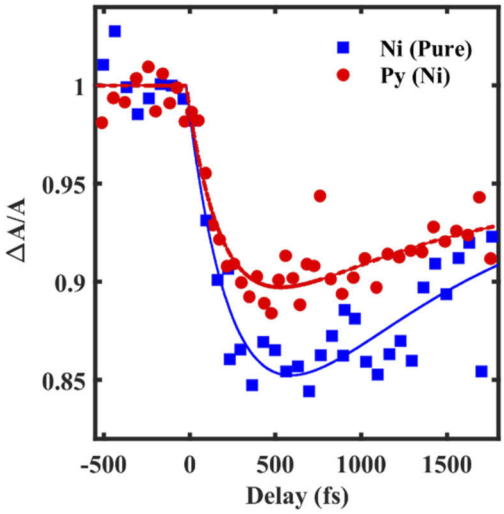


Fig. 5. Normalized asymmetry as a function of the time delay for Py (red, circle) and Ni (blue, square) samples measured at the $M_{2,3}$ absorption edges of Ni ($h\upsilon = 66.7$ eV).

To shed further light on our experimental findings and to estimate the demagnetization time quantitatively, the experimental data were fitted to the following expression [14]:

$$\frac{\Delta M}{M} = \left\{ A_1 - \frac{(A_2\tau_E - A_1\tau_{M/63}) \cdot e^{-\frac{t}{\tau_{M/63}}}}{\tau_E - \tau_{M/63}} - \frac{\tau_E(A_2 - A_1) \cdot e^{-\frac{t}{\tau_{M/63}}}}{\tau_E - \tau_{M/63}} \right\} H(t) \times \Gamma(t) \qquad (2)$$

Here H(t) is the Heaviside step function and τ_E and $\tau_{M/63}$ are the electrons-phonons thermalization time and the relaxation time from spins, respectively. A_1 represents the equilibrium temperature parameter, A_2 represents the initial electron temperature rise parameter and $\Gamma(t)$ is the XFEL pulse envelope determining the temporal resolution. Note that because of the very short pulses used, we do not use the $\Gamma(t)$ parameter to consider the experimental temporal resolution, except in Fig. 8 where we explicitly want to determine this resolution.

Since the range of delays that we could explore was limited, the fit parameters, in particular the demagnetization times, are not very accurate even though the curves we obtained are in very good agreement with the measurements. Indeed, the recovery time can be chosen almost arbitrarily leading to very different demagnetization times. To extract more meaningful information from these fits, we thus calculated the time for which the demagnetization reaches 63% ($1 - e^{-1}$) of its maximum, $\tau_{M/63}$. These values are reported in Table 1. The demagnetization time found for Ni (161 ± 30 fs) is slightly larger than the one found for Py (134 ± 30 fs) but within the error bar of our measurement, this cannot be completely ascertained.

Table 1. Ultrafast demagnetization fitting parameters obtained for Py (Ni) and Ni. The error bars are estimated by determining $\tau_{M/63}$ for several equally good fitting curves (with different fitting parameters) of the data and by rounding to the higher tens

Elements	Maximum demagnetization amplitude	$\tau_{M/63}$ (fs)
Ni	14.8%	161 ± 30
Py(Ni)	10.3%	134 ± 30

Optics EXPRESS

4. Transmission geometry results

Since the X-ray pulses at FLASH 2 are linearly polarized, it is impossible to use XMCD directly, even though it is the preferred X-ray technique to probe magnetization in transmission [15]. We therefore employ the resonant Faraday effect as a probe of the magnetization state of the samples [16,17]. Since linearly polarized light can be decomposed into two circularly polarized waves, having identical amplitude, but opposite helicity, the Faraday rotation can be explained as follows: when the right and left polarized components propagate through the medium, they exhibit different velocities which causes a phase shift between them, and thus, the Faraday rotation. In addition, the absorption coefficients of the two circularly polarized waves are different, therefore the amplitudes of their electric fields vary differently which changes the initially linearly polarized light into elliptically polarized light after transmission. The transmitted beam has therefore an additional small *s*-component compared to the pure incident *p*-polarized beam. We have recently demonstrated how to measure femtosecond magnetization dynamics using the Faraday effect at photon energies in resonance with absorption edges of elements [16].

The configuration of the experiment is sketched in Fig. 6. For this experiment, we have studied 30 nm thick Py and Ni samples. Both films were sputter deposited on chips consisting of a nine-by-nine grid of 50 nm thick Si_3N_4 windows. The windows are squares of 50 μm. The samples have been capped by a 5 nm Al layer to prevent them from being oxidized.

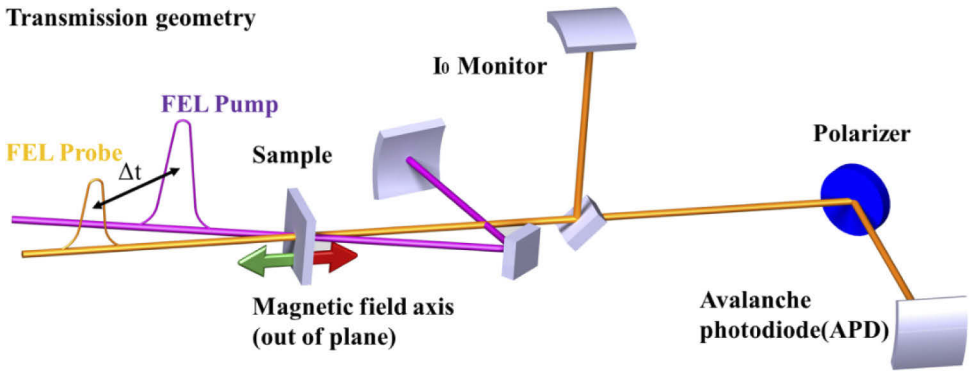


Fig. 6. Schematic diagram of the transmission setup showing, in addition to the split and delay unit, the out of plane magnetization of the sample (red and blue), the intensity monitors for pump and for probe, the polarizer (wide band multilayer) and the signal detector (APD).

In transmission geometry (see Fig. 6), the sample is set at normal incidence and magnetized out of plane by permanent ring magnets (maximum field of 350 mT, high enough to saturate the magnetization of the samples) to maximize the Faraday effect. To reverse the direction of the magnetic field, we use two sets of permanent ring magnets mounted in opposite direction on a vertical motorized stage. Behind the sample, the pump and probe beams diverge. The pump beam intensity is recorded on an X-ray photodiode after reflection on a gold coated mirror. Part of the probe beam is reflected upwards by a Si_3N_4 window and recorded by an APD. This window is set to an angle of incidence of 45°, close to the Brewster angle, and only reflects the *p*-component of the beam. Since the Faraday rotation is of the order of a few degrees at most, the *p*-component of the beam is mostly unaffected by the magnetic state of the sample, allowing us to measure the probe beam intensity even when the sample is excited by the pump. The fact that the I_0 monitors for pump and probe are placed after the sample provides a higher precision than in the reflection geometry since only the intensity of the light passing the 50 μm apertures of the sample is measured.

Optics EXPRESS

After the Si_3N_4 window, the probe beam is reflected by the polarizer which consists of a few repetitions Al/B4C multilayer mirror with a reflectivity higher than 10% in the 55 to 66 eV energy range purchased from OptiXfab. This polarizer mostly reflects the *s*-component of the XFEL pulses (the *s*-reflectivity is at least 200 times higher than the *p*-reflectivity), and its intensity is measured by an APD. The angle of incidence of the polarizer can be adjusted to optimize the amplitude of the magnetic signal by maximizing the extinction ratio (ratio between *s* and *p* reflectivity). The polarizer can also be rotated around the probe beam axis in order to move the reflection out of the horizontal plane. This allows us to work slightly out of the *p*-geometry which is essential to be able to see a difference between the two directions of magnetization [16]. Indeed, since the polarizer and detector are only sensitive to the magnitude of the *s*-component of the beam, both directions of magnetization give the same signal in a pure *p*-geometry. Working slightly out of the horizontal plane results in different signals for the two different magnetization directions, the difference between the two being proportional to the magnetization of the sample [16].

Finally, it has to be noted that the quality of all optics was increased for the transmission experiment. In particular, we used higher reflectivity coatings (an aperiodic Al/B4C multilayer with about 15% reflectivity between 52 and 68 eV from OptiXfab.) for the spherical mirrors. This allowed us to use very short pulses. Indeed, tuning the XFEL to deliver very short pulses reduces the pulse energy. To maintain a pump fluence sufficiently high to be able to excite the sample we need high reflectivity optics. For our experiment, we used an XFEL configuration known to deliver pulses shorter than 10 fs (based on streaking in-house machine experiments) with a pulse energy of about 10 μJ.

Figure 7 presents the normalized signals recorded after the polarizer for the two opposite magnetization directions around the Ni $M_{2,3}$ edges (between 63 and 71 eV). The Faraday effect is stronger where the two curves display the largest separation (around 65.5 eV). We therefore realized the time-resolved measurements on the Ni and Py samples at a photon energy of 64.7 eV (best compromise between the magnetic signal and the intensity on the photodiode). Figure 8 (a) shows the normalized transmitted intensity as a function of pump-probe time delay recorded for the Ni film for opposite direction of the sample magnetization. The time-resolved magnetization, *M,* is proportional to the difference between these two signals ΔI [16]. The sum of these two signals is not a straight line revealing a weak non-magnetic dynamic [17].

Figure 8(b) shows this signal normalized to the unpumped difference, ΔI_0. From this measurement, we can estimate a total time resolution of better than 15 fs for our experiment by looking at the initial drop of magnetization. Indeed, this drop occurs in an interval of 12 fs (three consecutive points each separated by 6 fs) showing that we can determine the onset of demagnetization with a precision better than 15 fs. Furthermore, fitting the graph of Fig. 8(b) with Eq. (2) we can determine the best Gaussian function (Γ(t) function in Eq. (2)) describing our data: the best results are obtained for a Gaussian with a 10 fs FWHM. Finally, the estimated pulse duration of less than 10 fs would yield at worst a time resolution of about 14 fs (the convolution of two 10 fs Gaussian profile is a 10 times square root of 2 Gaussian profile). All these evidences point to a sub-15 fs time resolution in this experiment. This time resolution is not far from the best time resolution achievable at attosecond harmonic sources – about 5 fs [4] – and the best that has yet been achieved for a femto-magnetism experiment at XFEL.

The implementation of the pump intensity monitor allows us to measure the pump intensity shot by shot. We can then extract fluence dependent demagnetization curves by sorting the different pump pulse intensities. Figure 9 (a) and (c) show the pump pulse intensity distribution obtained for Ni and Py, respectively. The double peak shape was the result of a XFEL instability that we could not get rid of during this beamtime (it usually is more gaussian). The data were sorted by low (green), average (blue) and high (red) pump fluence (Fig. 9). The fluence increases by a factor 1.6 from low to average and by a factor 1.5 from average to high. In both cases, Ni

Optics EXPRESS

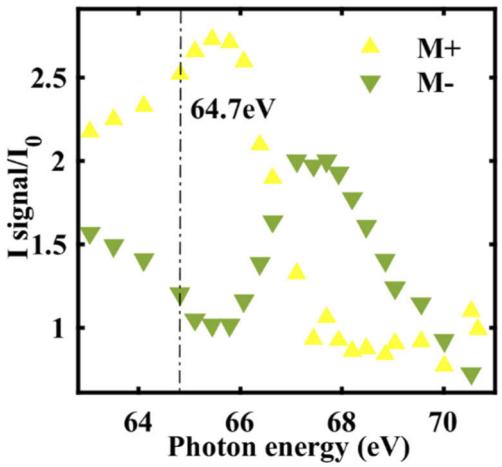


Fig. 7. Normalized signal after the polarizer as a function of photon energy recorded for the Ni sample around the Ni *M* edges. The signals for positive (yellow) and negative (green) magnetization have been recorded. At the crossing point of the curves recorded for opposite magnetization directions the Faraday rotation vanishes (at 66.9 eV). On the contrary the Faraday rotation is large between 64 and 66 eV (where the two curves are far apart). The further measurements have been done at 64.7 eV (black dashed line).

and Py, the maximum demagnetization scales linearly with the pump fluence. Even after data sorting, the signal to noise ratio is very good, especially for the Ni curves, demonstrating the very high potential of this technique, which allows to record multiple fluences in a single scan of about half an hour.

We used the same fitting procedure as in the reflection geometry to extract quantitative information from the curves. The results are reported in Table 2. The demagnetization time for Ni ranges from 142 to 166 fs and from 186 to 199 fs for Py suggesting that pure Ni demagnetizes faster than Ni in permalloy. This is confirmed by plotting both Ni and Py demagnetization traces on the same graph, for a similar maximum demagnetization of about 15% (Fig. 10 (a)) or alternatively for the same pump fluence (Fig. 11). The fitting result yields demagnetization times of 159 ± 20 fs for pure Ni and 193 ± 20 fs for Ni in Py for the former and 154 ± 10 fs for pure Ni and 202 ± 20 fs for Ni in Py for the latter. We also observe a small delay (about 25 fs) between the onset of the dynamics of Ni and Py (Fig. 10 (a)). It has to be reminded here that in our experiment time-zero (defined as a delay equal to zero between the pump and the probe) is set mechanically once and for all. However, the Ni and Py samples are not exactly in the same plane which prevents us from ruling out that this delay is not an artifact: a slight realignment of the beams was necessary between the two measurements.

Finally, we have measured the demagnetization dynamic of the Py sample at a photon energy of 53.6 eV at the M-edge of iron [10]. Comparison between this measurement and those performed at the nickel M-edge are shown in Fig. 10(b). Although the signal to noise ratio at the Fe edge is not as good as the one at the Ni edge, iron demagnetization dynamic (185 ± 30 fs) is similar to the one of nickel (196 ± 20 fs). Furthermore, we did not observe any delay between the onset of the demagnetization of Fe and Ni within the precision of our measurement. In that case, this observation is most probably free of any artifacts since the measurements have been made on the same sample, at the same sample position and without any modification of the optical path.

Optics EXPRESS

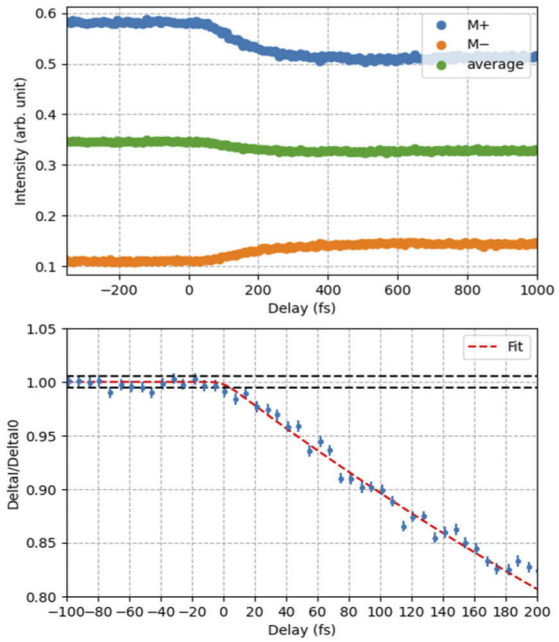


Fig. 8. (a) Normalized signal intensity recorded on the APD after the polarizer as a function of time delay for the Ni sample at a photon energy of 64.7 eV. A static out-of-plane magnetic field of 350 mT was applied in two opposite directions, M+ (blue) and M− (orange). The green curve is the average of the two time-resolved signals showing that they almost cancel each other. (b) Difference of the curves obtained for the two opposite magnetization directions, ΔI, normalized using the unpumped difference, ΔI_0 (obtained at negative delays), showing the magnetization dynamics of the sample (Alves *et al.*, 2019). The data points (blue) are separated by 6 fs and the two black dashed lines represent the standard deviation of the unpumped signal. The initial drop of magnetization occurs within two data points revealing a time resolution of about 12 fs. Furthermore, the best fits of the initial part of the magnetic transient (red dash) to Eq. (2) are obtained by using a Gaussian function ($\Gamma(t)$ in Eq. (2)) of about 10 fs FWHM, confirming our sub-15 fs time resolution.

Table 2. Summary of the data obtained on the 30 nm Ni and 30 nm Py thin films by probing with a photon energy of 64.7 eV, $(\Delta I/\Delta I_0)_{min}$ represents the maximum demagnetization. The error bars are estimated by determining $\tau_{M/63}$ for several equally good fitting curves (with different fitting parameters) of the data and by rounding to the higher tens

Sample and curve	Maximum demagnetization amplitude	$\tau_{M/63}$ (fs)
Ni (Low Intensity-Green)	13.3%	159 ± 20
Ni (Average Intensity-Blue)	22.1%	154 ± 20
Ni (High Intensity-Red)	29.3%	170 ± 20
Py (Low Intensity-Green)	5.3%	189 ± 20
Py (Average Intensity-Blue)	9.6%	205 ± 20
Py (High Intensity-Red)	13.9%	208 ± 20

Optics EXPRESS

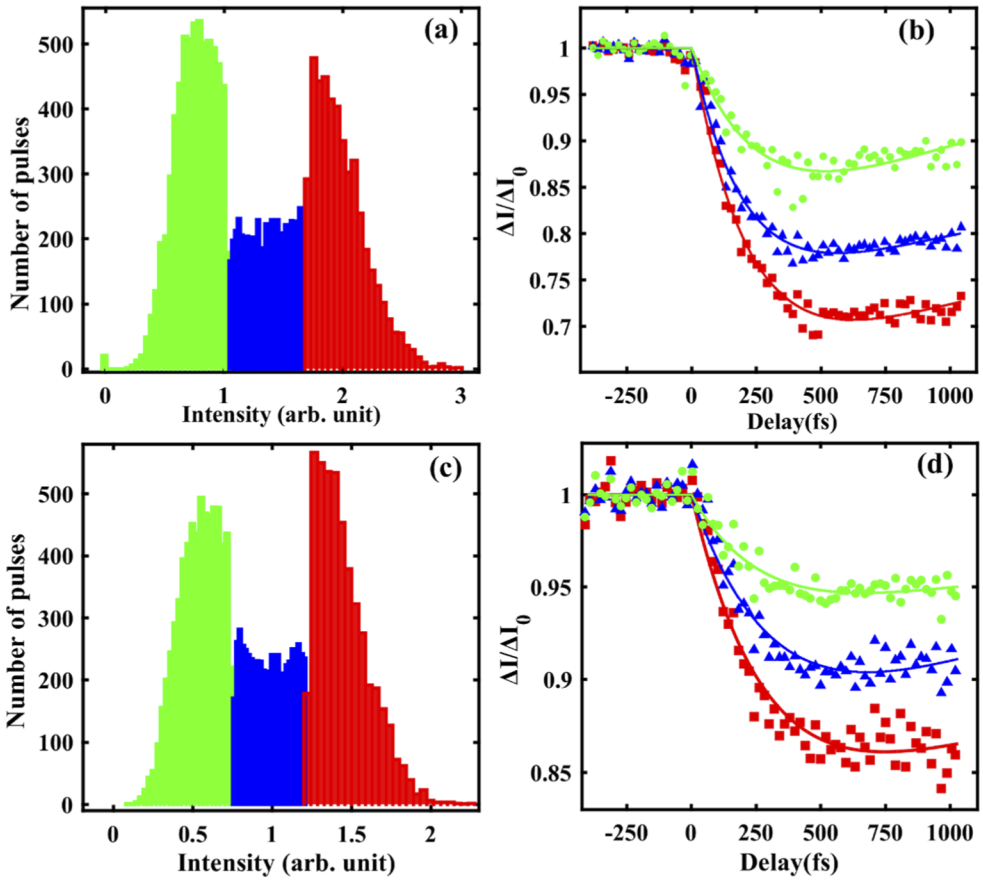


Fig. 9. (a) Pulse intensity distribution obtained during a delay scan on a Ni sample. The intensity has been sorted and grouped in low (green), average (blue) and high (red) pump fluence. (b) Demagnetization curves of a Ni sample obtained for these three pump fluences. (c) Pulse intensity distribution obtained during a delay scan on a Py sample. The intensity has been sorted and grouped in low (green), average (blue) and high (red) pump fluence. (d) Demagnetization curves of a Py sample obtained for these three pump fluences.

Optics EXPRESS

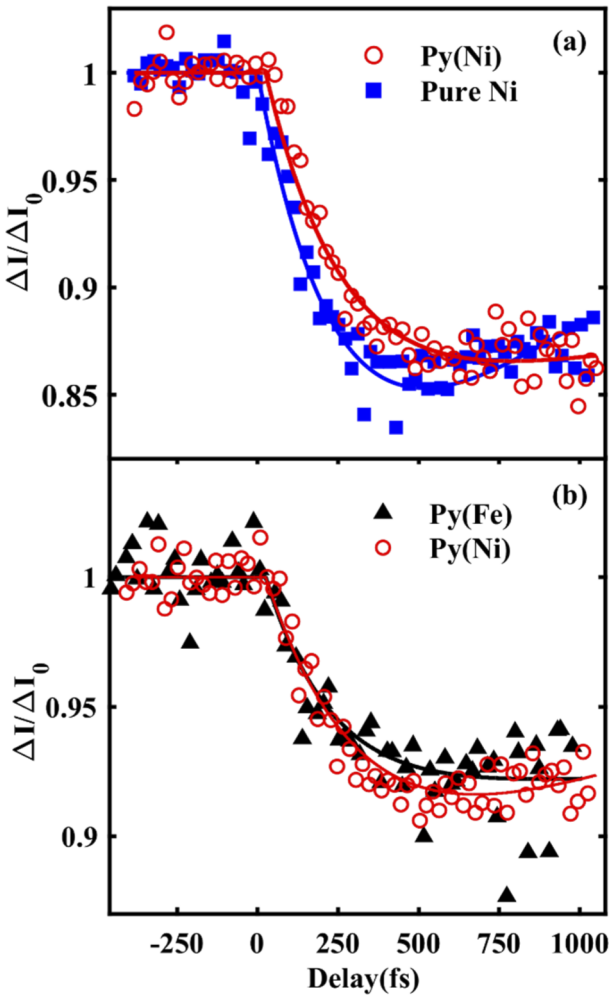


Fig. 10. (a) Element-specific demagnetization dynamics of Ni in pure Ni (blue square) compared to Ni in Py ($Ni_{80}Fe_{20}$) measured using the resonant Faraday effect. (b) Element-specific demagnetization dynamics of Ni in Py compared to Fe in Py obtained for a similar degree of demagnetization.

Optics EXPRESS

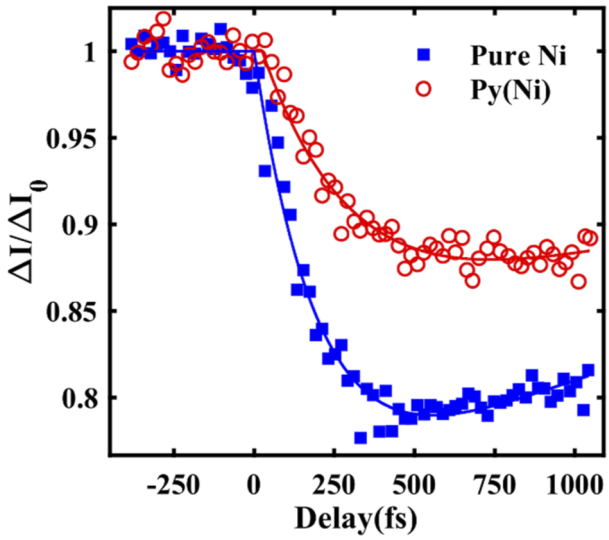


Fig. 11. The comparison between Py ($Ni_{80}Fe_{20}$) (red circle) and pure Ni (blue square) measured by Faraday effect with the same pump fluence range (from 1 to 1.5 in units of Fig. 9 (a) and (c)).

5. Conclusion

In summary, we have shown that a split and delay approach can be used to achieve the best time resolution possible at XFEL in ultrafast magnetization dynamics experiments. This technique can be implemented in different geometries providing a large choice of magneto-optical effects with linearly polarized radiation to probe the magnetization states of the different samples.

We have applied our setup to the study of the demagnetization dynamics of Ni and Py in both reflection and transmission geometry. The latter geometry yielded the best signal to noise ratio and time resolution (better than 15 fs) thanks to an improved normalization scheme allowing us to use the shortest XFEL pulses available. We found that pure Ni demagnetizes faster than Ni in Py as reported by Radu *et al*. [3], but in contrast to what has been shown in their work, we found that Fe and Ni have similar demagnetization dynamics in Py [18]. Given the different technical approaches (XMCD vs Faraday probing, different pumping wavelengths, different probing wavelengths etc., such studies need however more systematic investigations in order to provide a clearer picture about the microscopic demagnetization mechanisms active in multi-elemental alloys and heterostructures.

In reflection geometry, quantitative demagnetization time values were more difficult to ascertain but the demagnetization time of Ni in Py appears to be slightly shorter than the one of pure Ni. There are at least three possible explanations to this apparent discrepancy between the results of the two geometries: (i) the samples studied were not exactly identical (magnetic layers studied in reflection being 3 times thinner than the ones used in transmission); (ii) T-MOKE is a surface sensitive effect while the Faraday effect probes the magnetization of the entire thickness of the film; (iii)) the wavelength dependence of these two effects in Ni and Py could prevent us to accurately retrieved the magnetization transient yielding different results for different wavelengths [2,1]. All these different possibilities underline the need for more systematic studies with reproducible experimental conditions which are very difficult to obtain in femtosecond resolved spectroscopic experiments. The instrument we describe here has the potential to realize such systematic studies and we intend to continue our investigation of ultrafast demagnetization in Ni -

Optics EXPRESS

Fe systems while monitoring the exact influence of the probe wavelength and the magneto-optical effect used.

Funding. Investissements d'Avenir of Laboratoire d'excellence Physique Atomes Lumière Matière (ANR-10-LABX-0039-PALM); CNRS-PICS; UMAMI (ANR-15-CE24-0009); CNRS-MOMENTUM.

Acknowledgements. We thank the technical support of scientific and technical team at FLASH. In particular, the machine operators and coordinators. The authors are grateful for financial support received from the CNRS-MOMENTUM, the UMAMI ANR-15-CE24-0009, and the CNRS-PICS programs. Besides, I.R. acknowledges funding from the Federal Ministry of Education and Research (BMBF) through project 05K16BCA (Femto-THz-X) and from the German Research Foundation (DFG) through TRR227 (Ultrafast Spin Dynamics). This work has also benefited from the help of Investissements d'Avenir of LabEx PALM (ANR-10-LABX-0039-PALM) through the XUV10 project. I. R. acknowledges funding from the Federal Ministry of Education and Research (BMBF) through project 05K16BCA (Femto-THz-X)

Disclosures. The authors declare no conflicts of interest.

Data availability. The data that support the results of this study are available from the corresponding author upon reasonable request.

References

1. S. Mathias, C. La-O-Vorakiat, P. Grychtol, P. Granitzka, E. Turgut, J. M. Shaw, R. Adam, H. T. Nembach, M. E. Siemens, S. Eich, C. M. Schneider, T. J. Silva, M. Aeschlimann, M. M. Murnane, and H. C. Kapteyn, "Probing the timescale of the exchange interaction in a ferromagnetic alloy," Proc. Natl. Acad. Sci. **109**(13), 4792–4797 (2012).
2. S. Jana, R. S. Malik, Y. O. Kvashnin, I. L. M. Locht, R. Knut, R. Stefanuik, I. Di Marco, A. N. Yaresko, M. Ahlberg, J. Akerman, R. Chimata, M. Battiato, J. Söderström, O. Eriksson, and O. Karis, "Analysis of the linear relationship between asymmetry and magnetic moment at the *M* edge of 3*d* transition metals," Phys. Rev. Res. **2**(1), 013180 (2020).
3. I. Radu, C. Stamm, A. Eschenlohr, F. Radu, R. Abrudan, K. Vahaplar, T. Kachel, N. Pontius, R. Mitzner, K. Holldack, A. Föhlisch, T. A. Ostler, J. H. Mentink, R. F. L. Evans, R. W. Chantrell, A. Tsukamoto, A. Itoh, A. Kirilyuk, A. V. Kimel, and T. Rasing, "Ultrafast and Distinct Spin Dynamics in Magnetic Alloys," SPIN **05**(03), 1550004 (2015).
4. F. Siegrist, J. A. Gessner, M. Ossiander, C. Denker, Y. P. Chang, M. C. Schröder, and J. K. Dewhurst, "Light-wave dynamic control of magnetism," Nature **571**(7764), 240–244 (2019).
5. W. Helml, I. Grguraš, P. N. Juranić, S. Düsterer, T. Mazza, A. R. Maier, and C. Callegari, "Ultrashort free-electron laser x-ray pulses," Appl. Sci. **7**(9), 915 (2017).
6. R. Ivanov, J. Liu, G. Brenner, M. Brachmanski, and S. Düsterer, "FLASH free-electron laser single-shot temporal diagnostic: terahertz-field-driven streaking," J. Synchrotron Radiat. **25**(1), 26–31 (2018).
7. B. Mahieu, E. Allaria, D. Castronovo, M. B. Danailov, A. Demidovich, G. D. Ninno, S. D. Mitri, W. M. Fawley, E. Ferrari, L. Fröhlich, D. Gauthier, L. Giannessi, N. Mahne, G. Penco, L. Raimondi, S. Spampinati, C. Spezzani, C. Svetina, M. Trovò, and M. Zangrando, "Two-colour generation in a chirped seeded free-electron laser: a close look," Opt. Express **21**(19), 22728–22741 (2013).
8. E. Ferrari, C. Spezzani, F. Fortuna, R. Delaunay, F. Vidal, I. Nikolov, P. Cinquegrana, B. Diviacco, D. Gauthier, G. Penco, P. R. Ribič, E. Roussel, M. Trovò, J.-B. Moussy, T. Pincelli, L. Lounis, M. Manfredda, E. Pedersoli, F. Capotondi, C. Svetina, N. Mahne, M. Zangrando, L. Raimondi, A. Demidovich, L. Giannessi, G. De Ninno, M. B. Danailov, E. Allaria, and M. Sacchi, "Widely tunable two-colour seeded free-electron laser source for resonant-pump resonant-probe magnetic scattering," Nat. Commun. **7**(1), 10343 (2016).
9. A. A. Lutman, T. J. Maxwell, J. P. MacArthur, M. W. Guetg, N. Berrah, R. N. Coffee, Y. Ding, Z. Huang, A. Marinelli, S. Moeller, and J. C. U. Zemella, "Fresh-slice multicolour X-ray free-electron lasers," Nat. Photonics **10**(11), 745–750 (2016).
10. F. Willems, S. Sharma, C. v, K. Schmising, J. K. Dewhurst, L. Salemi, D. Schick, P. Hessing, C. Strüber, W. D. Engel, and S. Eisebitt, "Magneto-Optical Functions at the 3*p* Resonances of Fe, Co, and Ni: Ab initio Description and Experiment," Phys. Rev. Lett. **122**(21), 217202 (2019).
11. M. Schneider, B. Pfau, C. M. Günther, C. von Korff Schmising, D. Weder, J. Geilhufe, J. Perron, F. Capotondi, E. Pedersoli, M. Manfredda, M. Hennecke, B. Vodungbo, J. Lüning, and S. Eisebitt, "Ultrafast Demagnetization Dominates Fluence Dependence of Magnetic Scattering at Co *M* Edges," Phys. Rev. Lett. **125**(12), 127201 (2020).
12. A. Eschenlohr, "Ultrafast spin transport as key to femtosecond demagnetization," Nat. Mater. **12**(4), 332–336 (2013).
13. B. Koopmans, "Explaining the paradoxical diversity of ultrafast laser-induced demagnetization," Nat. Mater. **9**(3), 259–265 (2010).
14. G. Malinowski, F. Dalla Longa, J. H. H. Rietjens, P. V. Paluskar, R. Huijink, H. J. M. Swagten, and B. Koopmans, "Control of speed and efficiency of ultrafast demagnetization by direct transfer of spin angular momentum," Nat. Phys. **4**(11), 855–858 (2008).
15. G. Lambert, B. Vodungbo, J. Gautier, B. Mahieu, V. Malka, S. Sebban, and S. Stremoukhov, "Towards enabling femtosecond helicity-dependent spectroscopy with high-harmonic sources," Nat. Commun. **6**(1), 6167 (2015).
16. J. B. Kortright and S.-K. Kim, "(2000)," Phys. Rev. B **62**, (n.d.).

Optics EXPRESS

17. C. Alves, G. Lambert, V. Malka, M. Hehn, G. Malinowski, M. Hennes, V. Chardonnet, E. Jal, J. Lüning, and B. Vodungbo, "Resonant Faraday effect using high-order harmonics for the investigation of ultrafast demagnetization," Phys. Rev. B **100**(14), 144421 (2019).
18. L. Müller, C. Gutt, B. Pfau, S. Schaffert, J. Geilhufe, F. Büttner, J. Mohanty, S. Flewett, R. Treusch, S. Düsterer, H. Redlin, A. Al-Shemmary, M. Hille, A. Kobs, R. Frömter, H. P. Oepen, B. Ziaja, N. Medvedev, S.-K. Son, R. Thiele, R. Santra, B. Vodungbo, J. Lüning, S. Eisebitt, and G. Grübel, "Breakdown of the X-Ray Resonant Magnetic Scattering Signal during Intense Pulses of Extreme Ultraviolet Free-Electron-Laser Radiation," Phys. Rev. Lett. **110**(23), 234801 (2013).

90.16.59.12 {ts '2022-10-14 09:58:59'}